

Mechano-Chemical Processing of Diaspore Sample for Extraction and Synthesis of Gamma-Alumina and Potash Values

ASHWINI KUMAR,¹ SHREY AGRAWAL,¹ and NIKHIL DHAWAN ^{1,2}

1.—Extractive Metallurgy Laboratory, Department of Metallurgical and Materials Engineering, Indian Institute of Technology, IIT-Roorkee, Roorkee, Uttarakhand 247667, India.
2.—e-mail: ndhawan.fmt@iitr.ac.in

In this study, a diaspore sample is evaluated as a dual source of alumina and potash. The thermal treatment of diaspore with sodium hydroxide yielded alumina and potash values. Microwave heating resulted in enhanced diffusion with improved precipitate purity and recovery with a significant reduction in reaction time. The thermal treatment precipitate comprises alumina purity of 48% with a recovery of 49%. The mechanical milling route yields optimal conditions of 8 h milling followed by acid leaching in 2 M HCl at 50°C for 1 h with 20% and 45% potash and alumina extraction, respectively. The dissociation of the muscovite structure is crucial for high extraction values, and milling time was found to be the significant factor. The milling route at optimal conditions yielded an alumina precipitate with 89% purity with a surface area of 104.6 m²/g and a sylvinite-rich solution, which can be used in fertilizer application.

INTRODUCTION

Bauxite is the primary ore employed for alumina production.¹ The increasing demand for aluminum metal and other allied applications such as refractory material, abrasive, and catalyst leads to high alumina consumption.²⁻⁴ The available bauxite reserves are inadequate to meet the growing demands, and industries rely on alternative non-bauxite sources for production. The annual aluminum production in India reached 3.4 million tons in 2018, with an annual growth of 17% and alumina production of 6.12 million tons.⁵ The primary aluminum minerals in bauxite ore are gibbsite (*c*-Al(OH)₃), boehmite (*c*-AlO(OH)), diaspore (*a*-AlO(OH)), and clay minerals such as kaolinite, halloysite, and aluminous goethite.⁶ The bauxite ore with high diaspore content is not considered ideal for alumina production using Bayer's process because of the low Al-to-Si ratio, considerable red mud generation, high temperature, and pressure requirements for processing.⁷ The alternative processing route employed for alumina recovery from diasporic bauxites, nepheline syenite, and kaolin can be broadly classified into a hydrometallurgical

route involving acid leaching and a combined pyro- and hydrometallurgical route. Aluminum-bearing phases exist in different forms such as *g*, *c*, *d*, *h*, *b*, *j*, *v*, and *a*-alumina crystalline structures, where *c*-alumina is an important structure having applications such as catalysts, composite structures, and thermal insulation in oil hydrogenation, chemical synthesis, petroleum refining, and aerospace industries.⁸⁻¹⁰ High-purity *c*-alumina is commercially prepared from aluminum precursors using chemical deposition and hydrothermal methods.¹⁰⁻¹² The previous studies conducted on the synthesis of *c*-alumina reported a specific surface area of 110–150 m²/g.¹³ The scarcity of soluble potash resources such as sylvinite, sylvite, and carnallite has pushed research efforts toward the processing of silicate minerals such as sericite-muscovite, glauconite, feldspar, and nepheline syenite containing 6–12% K₂O and 30–50% Al₂O₃ for the recovery of alumina and potash.¹⁴⁻¹⁶ Table I shows the alternative alumina extraction processes reported for diasporic bauxite and non-bauxite sources.

Incorporation of microwaves in mineral processing problems is gaining much attraction because of its unique characteristics such as noncontact, rapid,

Table I. Literature review of alumina extraction by hydro-thermal treatment from Al resources

| S. no. | Key findings | Al source and location | References |
|--------|--|---|-------------------------------|
| 1 | Calcination followed by acid leaching at optimal conditions of 550°C roasting temperature, 1.2 M H ₂ SO ₄ with liquid-to-solid ratio of 9:1 at 70°C for 2 h, yielded 30.3% K and 47.3% Fe | Low-grade bauxite (Henan, China) | Li et al. ¹⁷ |
| 2 | High-temperature calcination followed by H ₂ SO ₄ leaching resulted in 95.1% alumina extraction and 26.6% iron dissolution Optimum conditions: calcination of the clay at 750°C for 30 min followed by leaching in 3 M H ₂ SO ₄ using an acid-to-clay ratio of 4:5 at 100°C for 120 min | Aluminum clay mineral (Lampang, Thailand) | Numluk et al. ¹⁸ |
| 3 | Calcination of kaolin-NaCl mixture followed by acid leaching and precipitation yielded precipitate having 79.28% alumina. The optimal conditions were roasting at 700°C and leaching at 140°C for 3 h 45 min with 40% H ₂ SO ₄ | Kaolin (Jordan) | Ibrahim et al. ¹⁹ |
| 4 | High-temperature HCl leaching of nepheline at 6 M, 2 h, 70°C and L:S of 20 yielded 82% alumina. The synthesized alumina has nanocrystalline morphology with a surface area of 39.1 m ² /g | Nepheline syenite (Azarshahr, Iran) | Chitan et al. ¹⁰ |
| 5 | Acid leaching of powdered Al cans with HCl resulted in AlCl ₃ , which is transformed to Al(OH) ₃ using NH ₄ OH/NaOH. The precipitate is calcined to form α -alumina having a surface area of 174–204 m ² /g | Aluminum can | Adans et al. ²⁰ |
| 6 | Diasporic bauxite powder was calcined at 900°C for 60 min with CaO and Na ₂ CO ₃ followed by water leaching for 15 min at 50°C with 85.04% extraction | Diasporic bauxite (Yalvac, Turkey) | Pehlivan et al. ²¹ |
| 7 | Raw slurry of diasporic bauxite ore, Na ₂ CO ₃ , and Ca(OH) ₂ exhibited high microwave absorption characteristics, reaching 800°C after only 20 min at constant microwave power of 1.0 kW. Al extraction from the microwave-roasted product at 800°C for 45 min was 82.24%, while the leaching rates of Na and Si were 90.2% and 8.4%, respectively | Diasporic bauxite (China) | Le et al. ²² |

selective, volumetric, and bulk heating with efficient energy transfer.²³ Microwave heating of diasporic bauxite ores reported improved aluminum extraction, reduced digestion time, and temperature compared with the conventional heating method.²² The dielectric property of the material governs the interaction between microwaves and minerals, of which the ability of a material to convert absorbed microwave energy into thermal energy is given by imaginary permittivity.²⁴ The dielectric properties of bauxite ore investigated at 915 MHz indicate the boehmite mineral in the ore showed high permittivity up to 330°C and decreases beyond that due to α -alumina formation by dehydroxylation. On further increasing the temperature up to 1000°C, the imaginary permittivity value reaches 0.29 compared with 0.06 at 25°C.²⁴

This study aims to develop a process route to utilize diasporic sample as a dual source of alumina and potash. The recovery of potash from alumina-rich sources such as diasporic or the mica family can be beneficial for agriculture-based economies such as Brazil and India that do not have sustainable potash sources and rely on imports. An attempt is made to break the stable structure of diasporic and recover both alumina and potash in a suitable form. The alkali thermal treatment involving conventional heating, microwave heating and mechanical

activation is investigated as a pre-treatment step followed by acid leaching. An overall comparison is also made between the processing routes followed.

MATERIALS AND METHODS

The diasporic sample used in this study was procured from a working mine in Jhansi district, Madhya Pradesh, India. The as-received sample was crushed stage-wise using a jaw and roll crusher followed by milling in a laboratory-scale ball mill to obtain the desired particle size ($\sim 100 \mu\text{m}$). The elemental composition of the representative sample was determined using standard chemical analysis. The mineralogical composition and phase alterations during the processing were investigated using x-ray diffraction (XRD) at a 2 θ angle of 5–80° at a step size of 2°/min. The semiquantitative analysis was performed to determine the degree of crystallinity and was calculated by the formula (I/I_0)⁹ 100 where I_0 and I correspond to the peak intensity of the phase before and after treatment, respectively.¹⁶ The structural alteration and morphology of the products were investigated by scanning electron microscopy (SEM), and elemental composition was determined by electron-dispersive spectroscopy (EDS). The effect of milling on particle size and surface area was quantified using the BET

surface area because of the very fine particle size. Aluminum and potassium dissolutions were determined using inductively coupled plasma mass spectroscopy (ICP-MS) and a flame photometer (FPM).

The experimental procedure comprises alkali thermal treatment, and mechanical milling as shown in Fig. 1d. In alkali thermal treatment, the sample was heat-treated with sodium hydroxide for a predetermined time and temperature. The excellent microwave absorbing and heating ability of sodium hydroxide was exploited by incorporating microwaves as a heating source.²⁵ The heat-treated mass was water leached for the separation of water-soluble phases. In the mechanical milling route, the sample is loaded in a tungsten carbide jar for 2–8 h at a fixed revolution speed of 300 rpm and ball-to-powder ratio of 10:1 in a planetary ball mill (Retsch, PM100) based on the scoping experiments. The water leach residue of the alkali thermal treatment and the milled product was further dissolved in hydrochloric acid for 1 h, and a solid-to-liquid ratio of 1:25 was kept constant. The aluminum values in the solution were precipitated at neutral pH, and the filtered solution was analyzed for K content.¹⁶

The precipitate was calcined at 1000°C for 1 h for the conversion of the boehmite phase to α -alumina, followed by surface area measurement.

RESULTS AND DISCUSSION

Characterization

The bulk composition of the representative sample comprises SiO_2 , Al_2O_3 , and K_2O of 40.1, 50.4, and 6.3%, respectively, with traces of Fe_2O_3 and TiO_2 . The XRD analysis of the sample shown in Fig. 1a depicts the muscovite and diaspore phase of approximately 40% and 60%, respectively. The muscovite phase belongs to the mica family of aluminosilicate rocks and has similar morphology to the illite phase resulting in overlapping of x-ray diffraction peaks, making it difficult to differentiate. The prime difference is the higher silicon and iron content in the illite compared with the muscovite phase. The SEM micrograph is shown in Fig. 1b and reflects the dispersed particle morphology with an average particle size of < 30 microns with 21% Al and 5% K. The optical micrograph of diaspore under the cross-polarized light is shown in Fig. 1c. The lathe shape structure with multiple interference

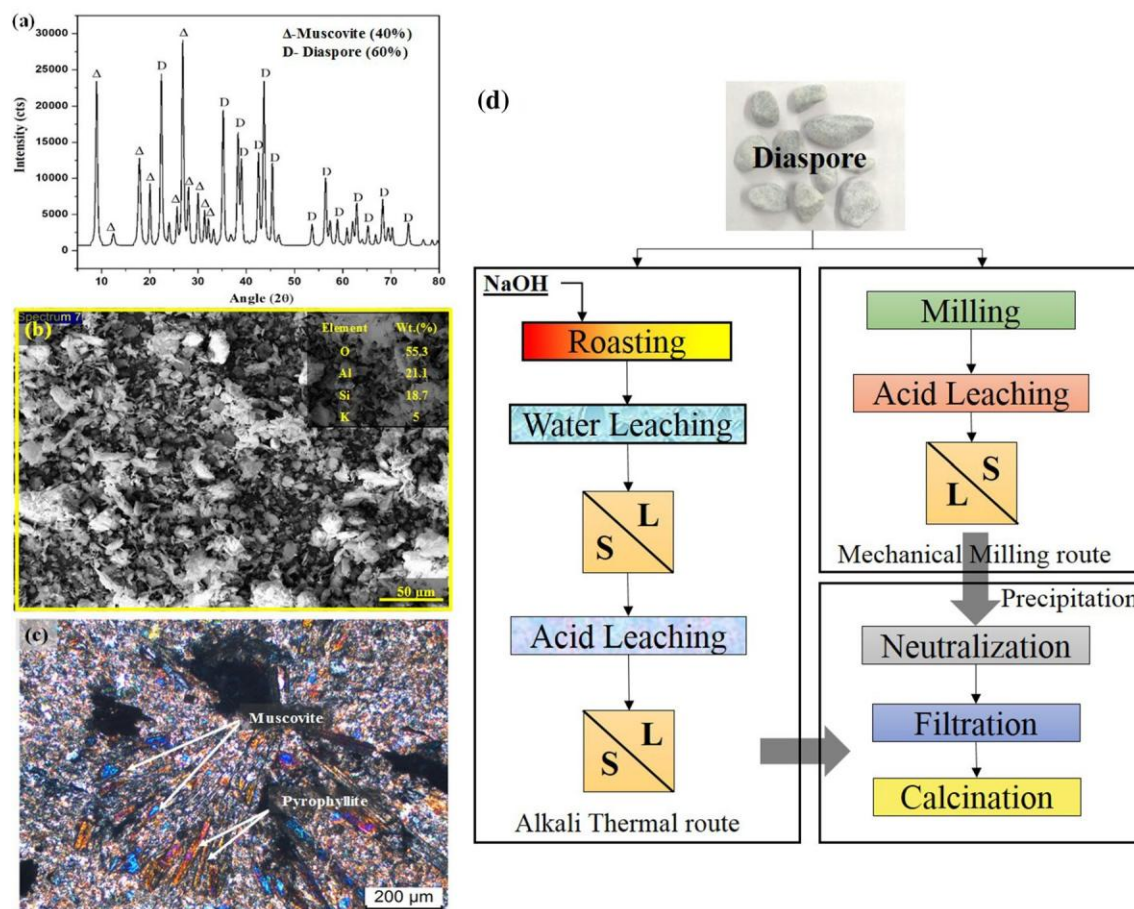


Fig. 1. (a) XRD spectra, (b) SEM micrograph, and optical microscopic image in (c) cross-polarized light and (d) process flowsheet for extraction of both alumina and potassium values.

colors suggests pyrophyllite, whereas the altered surface with multiple interference colors depicts muscovite (mica group). The thermogravimetric plot of the diaspore-NaOH mixture is shown in Fig. 2a. The graph depicts three significant temperature slopes in the range of 95–125°C, 270–325°C, and 350–600°C at 50% and 100% NaOH dosage, and the corresponding DT curve showed similar exothermic peaks at 90°C, 140°C, 280°C, and 330°C in both mixtures. The first stage of decomposition at 90–140°C is attributed to the moisture removal, and the second stage, 270–280°C, is because of the evolution of hydroxylates and vaporization of chemically bonded water molecules. The third stage of decomposition at 330°C is because of the melting of sodium hydroxide.

Reaction Kinetics

The diffusion of sodium hydroxide flux in the diaspore structure and corresponding breakage of the stable muscovite and diaspore phase depends primarily on the temperature. Determination of reaction kinetics and activation energy is crucial for maximizing the product yield and designing an efficient process. The theoretical activation energy was determined using thermogravimetric analysis via the Coats-Redfern method; according to Eq. 1, the plot between $\ln \left[\frac{a}{1-a} \right] \exp \left[\frac{E}{RT} \right]$ and $1-T$ yielded an activation energy from its slope at different thermal conditions.²⁶ Here, a is the reaction conversion degree, and it is quantified as the ratio of weight loss at a particular temperature to total weight loss incurred during the reaction, and n is the reaction order governing the decomposition kinetics. The average value of activation energy is

131.3 kJ mol⁻¹, and the energy value does not vary with NaOH dosage.

$$\frac{da}{dT} \frac{A}{b} \exp \frac{-E}{RT} \delta 1 - a b^n \quad \delta 1 b$$

Calcination Treatment

According to the stoichiometric ratio and mineral composition, the muscovite and diaspore contribute 25% and 75%, respectively, of the total Al₂O₃ content, and muscovite phase is the only source of potash in the ore. Calcination involves the phase transformation of diaspore and dehydroxylation of the muscovite phase. The calcination effect is envisaged by using HCl leaching through the determination of liberated potash content during phase transformation. According to TG analysis, the significant weight loss in the feed occurs in the temperature range of 490–650°C. Figure 2b shows the XRD plot of the calcined diaspore sample at 650°C and 1000°C and acid leach residue of the calcined mass. It is observed that the corundum (α -Al₂O₃) phase increases with an increase in calcination temperature; consequently, the diaspore phase disappears. The chemically bonded water molecules with diaspore and muscovite are released and transform into the corundum and dehydrated muscovite phase, respectively. A trace amount of nepheline formation was also observed from the XRD at low concentration. The XRD analysis reveals that the calcination treatment was ineffective in the dissolution of the muscovite phase and thus resulted in lower dissolution. The

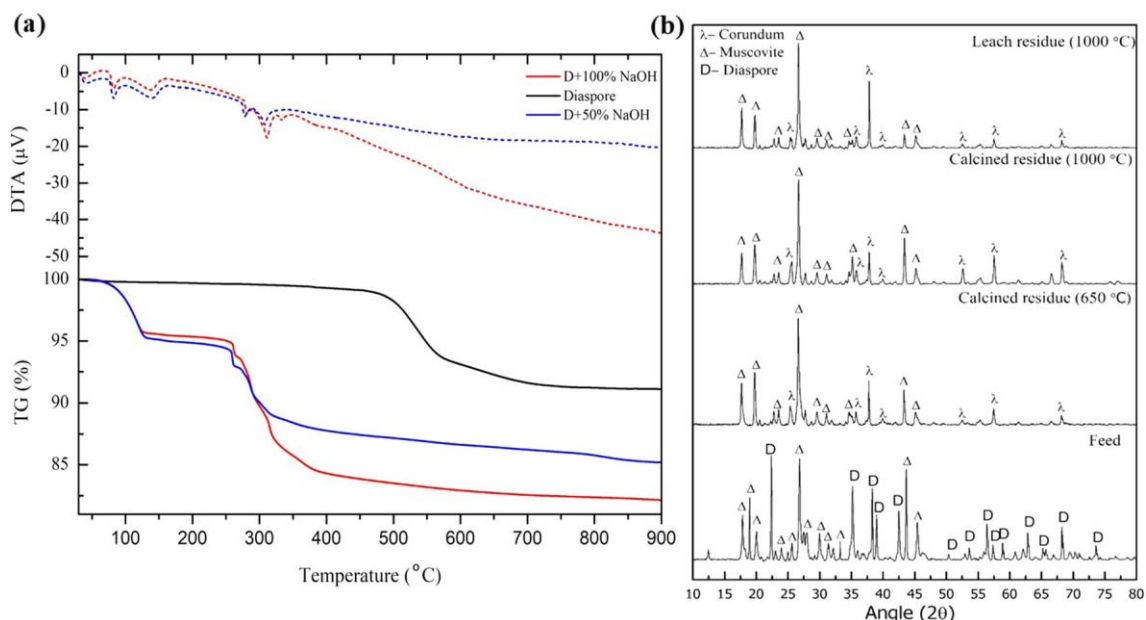


Fig. 2. (a) TG and DT plot of the diaspore-NaOH mixture at different temperatures and (b) XRD analysis of the calcined diaspore at 650°C and 1000°C and leach residue.

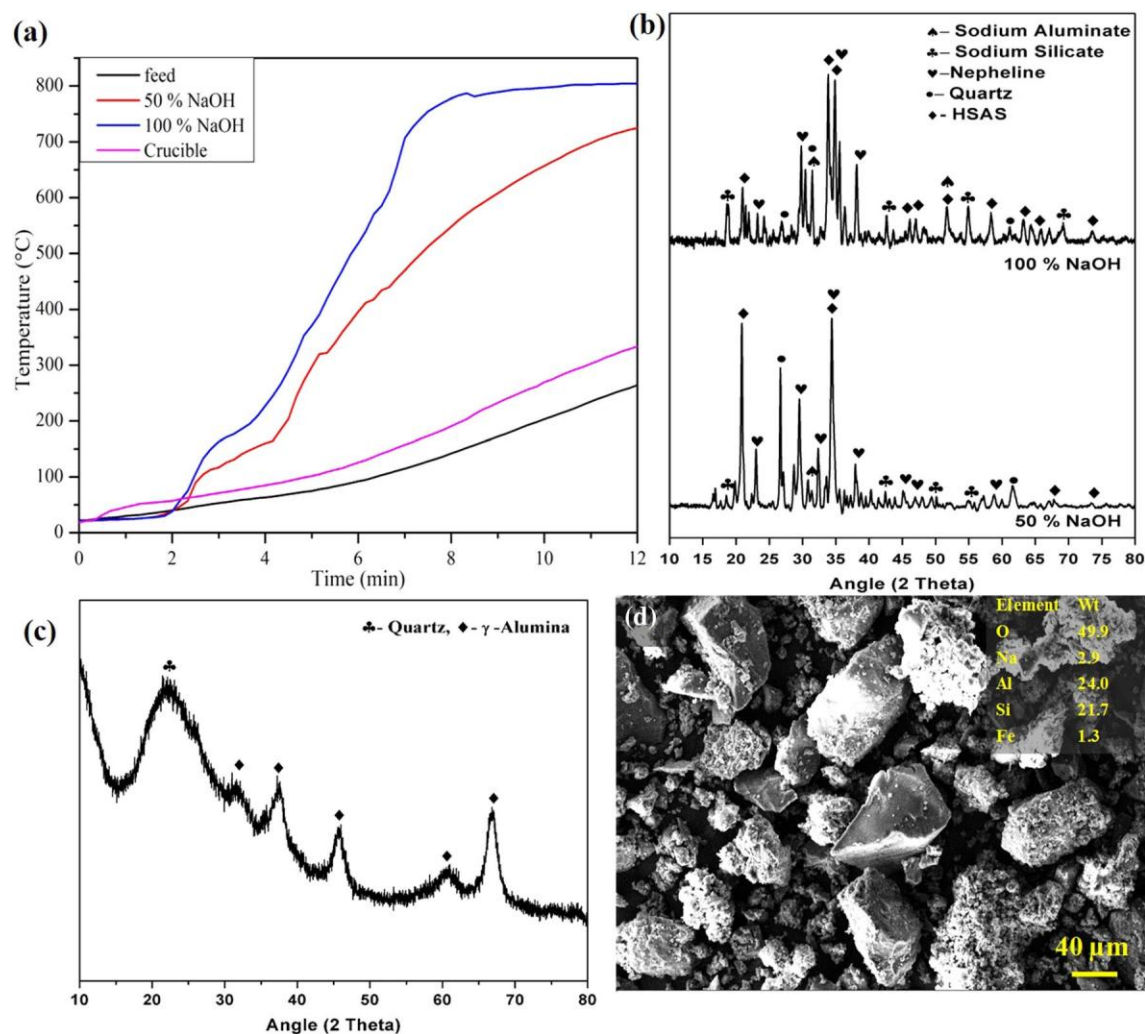


Fig. 4. (a) Time-temperature plot of microwave exposure at 800 W, (b) XRD plot of microwave-treated sample at 50% and 100% NaOH, (c) XRD, and (d) SEM-EDS analysis of the calcined precipitate of the microwave route (800 W, 10 min, 100% NaOH).

and the maximum temperature reached $\sim 800^{\circ}\text{C}$ in 8 min and saturated on prolonged exposure. The heating rate was consistent in 100% NaOH mixture over the temperature range of 250–700°C and is approximately 120°C/min.

On the contrary, the temperature of the 50% NaOH mixture showed a continuous decreasing heating rate, and the maximum value of 90°C/min was achieved within 250–400°C. The reported weight loss after 10 min exposure in the 1:1 NaOH-diaspore mixture is 14.3% and 10.9% in a 2:1 ratio. The corresponding weight loss as per thermogravimetric analysis was reported in the temperature range of 320–340°C and 370–390°C for 50% and 100% NaOH, respectively. The significantly faster heating rate in microwave heating compared with muffle furnace heating resulted in a rapid rise in temperature; consequently, the underlying chemical reaction was carried out at relatively higher temperatures resulting in lower activation energy with faster decomposition. The XRD plot of

microwave-treated products of 50% and 100% NaOH shown in Fig. 4b depicts complete dissociation of muscovite and diaspore with the formation of insoluble HSAS, soluble sodium aluminate, and sodium silicate phase. The phases formed were similar to the conventional heating process; however, the phase fraction varied, and semiquantitative phase analysis indicated that the sodium silicate formation was greater with higher flux. The morphological and phase characterization of the calcined precipitate corresponding to the 100% NaOH mixture is shown in Fig. 4c and d. The precipitate obtained with 100% NaOH comprises alumina purity of 48.2% with 49% recovery and 45.7% with 47.5% recovery for 50% NaOH. The broad peaks in the XRD plot at 31.92°, 37.60°, 45.86°, and 67.03° correspond to the formation of crystalline γ -alumina as confirmed by JCPDS file no. 29-63.³⁰ There was no distinguishable difference in the precipitate morphology in either the muffle

furnace or microwave route, and XRD indicates it comprises γ -alumina and amorphous silica.

Mechanical Milling

The alkali treatment resulted in silica accumulation in the final precipitate, thereby leading to low alumina purity with low recovery (~49%) in both routes. Direct acid leaching of diaspore samples yielded a maximum dissolution of 4% depicting minimal dissociation of the diaspore structure. The breakage of the muscovite phase is imperative to achieve high alumina and potash recovery; therefore, planetary ball milling was pursued, followed by acid leaching. Figure 5a shows the XRD plot of the milled product and indicates effective breakage of the muscovite phase with milling, and approximately 90% loss in crystallinity was achieved in 6 h milling. Muscovite is a relatively softer phase having Mohr's hardness of 2–3 compared with 6.6–7 of diaspore. Figure 5b and c shows the effect of milling time on the surface area and crystallinity of the sample, respectively. The surface area increases up to 6 h with a maximum value of 48.4 m²/g and decreases with extensive milling because of agglomeration of very fine particles. The variation in crystallinity degree with milling time indicates that a significant breakdown of the muscovite phase occurred during the initial period of milling (4 h) and further dissociation saturated at 6 h milling

with ~90% crystallinity loss depicting structure breakage.

Planetary ball milling followed by acid leaching, was optimized using a Box-Behnken statistical design. The effect of milling time, acid concentration, and leaching temperature were investigated and optimized. The primary objective of the statistical design is to maximize the Al₂O₃ and K extraction, and the investigated experimental design conditions with extraction values are shown in Fig. 6a.

According to the design results, K and Al₂O₃ extraction was in the range of 51–71% and 30–45%, respectively. The optimal conditions derived in the investigated range of parameters were 8 h milling followed by leaching at 2 M HCl, 50°C for 1 h. According to statistical analysis, the experimental values of K and Al₂O₃ extraction were best fitted to a modified quadratic model. The statistical parameters, the F value and p value, of the modified quadratic model for K extraction are 49.05 and 0.0002, respectively, and for Al₂O₃ extraction are 42.80 and < 0.001, respectively, indicating statistically significant models. In both cases, the milling time and acid concentration were dominant parameters governing the extraction process, whereas the leaching temperature was the least influential parameter. The empirical formulas derived from the above model for sequential Al₂O₃ and K extraction are, respectively, shown in Eqs. 3 and 4.

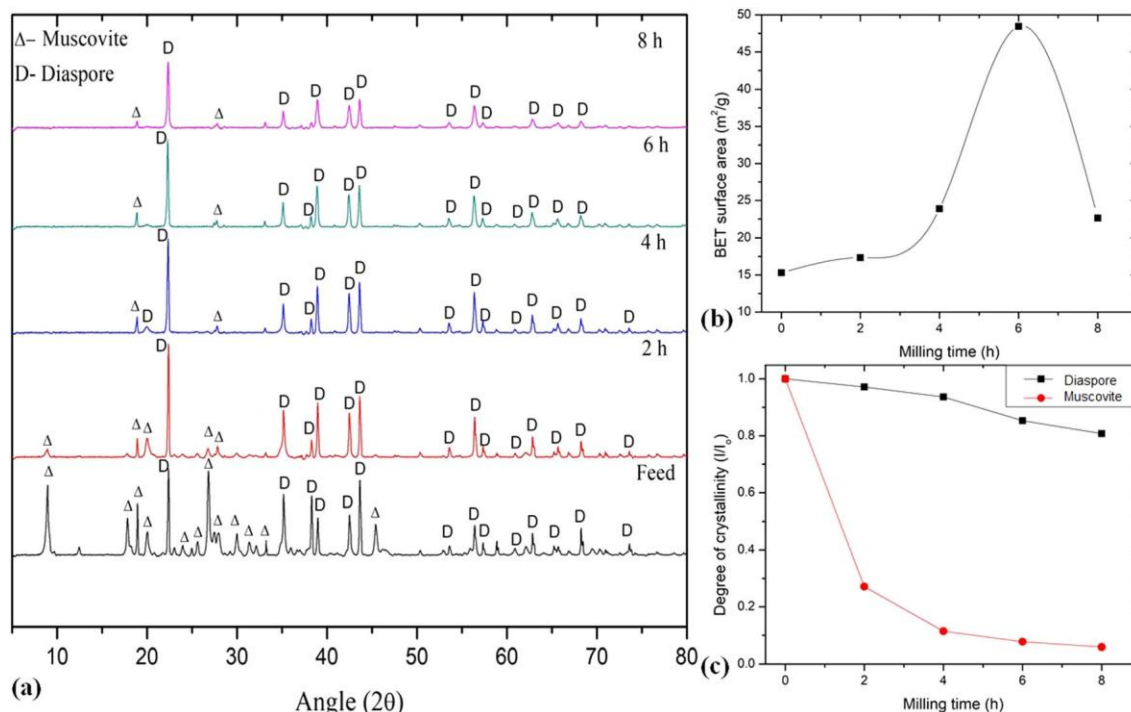


Fig. 5. (a) XRD plot (b) effect of milling time on the surface area, and (c) variation in crystallinity degree.

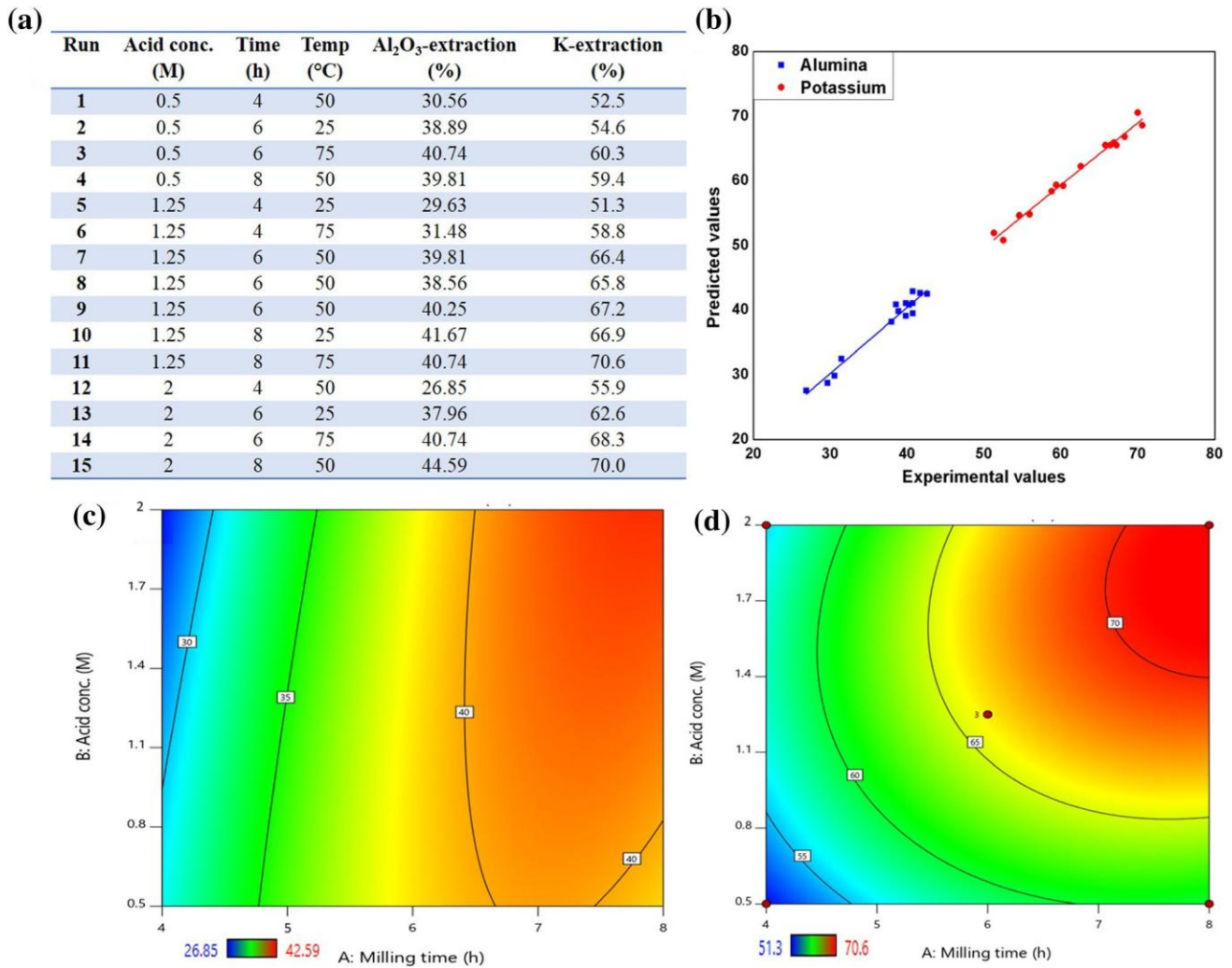


Fig. 6. (a) Experimental design conditions and responses, (b) actual versus predicted extraction values, and contour plots of influential factors for (c) alumina, and (d) potassium extraction.

K - extraction

$$\begin{aligned} & \frac{1}{4} - 2:852 \beta 11:760 \times \text{Milling time} \delta h \beta \\ & \beta 13:633 \times \text{Acid conc} \delta M \beta 0:404 \\ & \times \text{Temperature} \delta ^\circ C \beta 1:20 \times \text{Milling time} \\ & \times \text{Acid concentration} - 0:019 \times \text{Milling time} \\ & \times \text{Temperature} \beta 0:001 \times \text{Acid Concentration} \\ & \times \text{Temperature} - 0:774 \times \text{Milling time}^2 \\ & - 6:320 \times \text{Acid Concentration}^2 - 0:002 \\ & \times \text{Temperature}^2 R^2 \frac{1}{4} 0:988 \end{aligned}$$

Al₂O₃ - Extraction

$$\begin{aligned} & \frac{1}{4} - 3:770 \beta 13:376 \times \text{Milling time} \delta h \beta - 6:342 \\ & \times \text{Acid conc} \delta M \beta - 0:097 \times \text{Temperature} \delta ^\circ C \beta \\ & \beta 1:081 \times \text{Milling time} \times \text{Acid concentration} \\ & \beta 0:012 \times \text{Acid Concentration} \times \text{Temperature} \\ & \beta 0:986 \times \text{Milling time}^2 - 0:431 \\ & \times \text{Acid Concentration}^2 - 0:001 \\ & \times \text{Temperature}^2 R^2 \frac{1}{4} 0:982 \end{aligned}$$

δ3β

δ4β

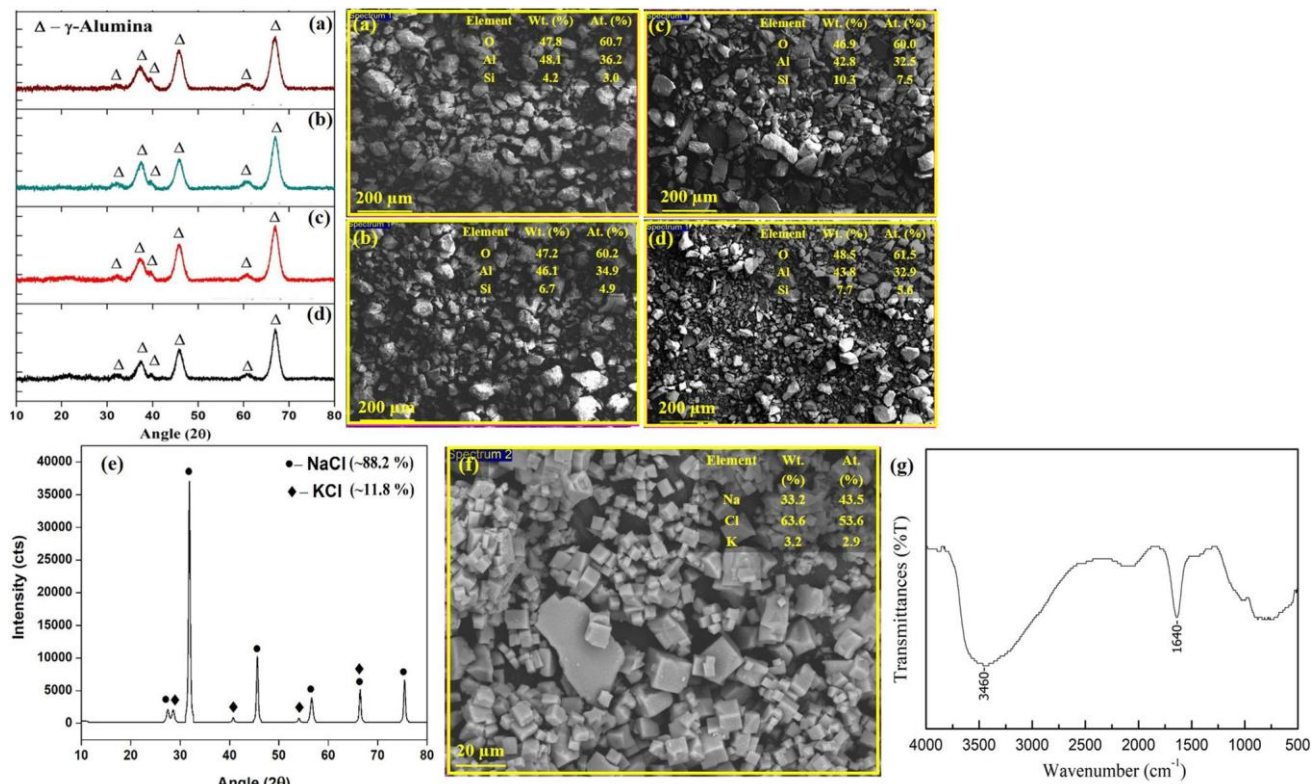


Fig. 7. XRD spectra and SEM micrograph of the final precipitate at different experimental conditions: (a) 8 h, 2 M, 50°C, (b) 8 h, 1.25 M, 50°C, (c) 6 h, 1.25 M, 50°C, (d) 6 h, 0.5 M, 50°C, (e) XRD plot, (f) SEM micrograph of the crystallized leach solution containing potassium, and (g) FTIR of the alumina precipitate.

Figure 6b shows good agreement between the actual experimental values and the predicted values for both responses. Figure 6c and d. shows the contour plots for Al₂O₃ and K extraction, respectively, with the influential parameters. It can be inferred from the plot, for high alumina extraction, a moderate to high acid concentration was desirable at moderate temperature; a high acid concentration and temperature are desirable for the maximum K extraction whereas the prolonged milling time was desirable for both extractions. Figure 7a, b, c, and d shows the XRD and SEM analysis of the final precipitate at different experimental conditions. The XRD plot depicts γ -alumina formation in all the experiments, and the precipitate purity is evaluated by EDS analysis. As expected, the Al content in the precipitate decreased insignificantly by ~2% on reducing the HCl concentration and 4% with a reduction in the milling duration. The atomic wt.% of the Al, Si, and O determined by EDS analysis indicates the formation of alumina and silica, and the molar ratio of alumina to silica in the optimal precipitate is 18:1. The Al₂O₃-to-SiO₂ ratio in the precipitate increased from 1.25 to approximately 10.2, with negligible K content. The alumina purity of the precipitate is 89.8%, with 44.6% recovery with a process yield of 27%. The obtained precipitate contains < 10% SiO₂, and approximately 89% Al₂O₃ can be used as a feedstock for

metallurgical-grade alumina production in Bayer's process. The low silica content prevents the formation of the desilication product and renders the Bayer process feasible. The surface area of the γ -alumina precipitate is 104.7 m²/g suggesting the formation of a nanocrystalline precipitate and is in close approximation to the previously reported values.^{15,20} The potash values recovered after the crystallization of the leach solution shown in Fig. 7e and f show the XRD and SEM micrograph of the crystals. The cubical crystals reflect the formation of sylvinit (KCl) and sodium chloride (NaCl), which is also confirmed by the XRD analysis. The leach solution can be further processed by fractional sublimation to remove the sodium impurities and recover potash values. The obtained FTIR plot shown in Fig. 7g is similar to the previously reported plots of nanocrystalline γ -alumina, and the broad band at 3460 cm⁻¹ and weak band at 1640 cm⁻¹ are because of the adsorbed water molecules.³¹

The techno-economic assessment of the process suggests that during alkali thermal treatment, approximately 12.15 kg of diaspor with ~ 14.2 kg of sodium hydroxide flux and 7.45 kg HCl is consumed for the synthesis of 1 kg γ -alumina. In contrast, in the mechanical milling route, the specific consumption of diaspor, sodium hydroxide, and HCl is 4.25 kg, 2 kg, and 3.5 kg, respectively,

reflecting a saving of 65% raw material resources and 66% consumables in addition to 45% alumina and 70% K extraction. Apart from the alumina-rich product, the potassium values recovered in the KCl form have a potential application in the fertilizer industry. Compared with the conventional Bayer processing for alumina production, the current investigated process is suitable for high silica aluminum sources such as diasporite because of the strict requirement for low silica content ($< 8\%$) in the ore for the Bayer process. Also, the recirculation of alkali in the liquor reduces the alkali consumption, which will be the focus of future work on the current process.

CONCLUSION

The present study investigates a diasporite sample containing 50.4% alumina and 6.3% potash as a potential dual source of extraction for both Al and K. The direct acid leaching of diasporite was found ineffective and resulted in poor dissolution. Alkali heat treatment and mechanical milling routes resulted in dissociation of the diasporite structure with simultaneous recovery of α -alumina and potash. The formation of aluminosilicate phases, such as nepheline and sodium aluminosilicate, during heat treatment enhances the dissolution rate in acid leaching. However, employing sodium hydroxide during the thermal treatment resulted in the accumulation of silica values in the precipitate and led to the formation of a low-purity α -alumina precipitate. The incorporation of microwaves induces volumetric and efficient heating, which leads to a rapid heating rate of approximately $120^\circ\text{C}/\text{min}$. The precipitate obtained by the conventional heating route contains 38% Al_2O_3 with 43.3% recovery, and the microwave-heated precipitate contains 48.2% Al_2O_3 with 49% recovery. Mechanical milling was found more efficient for α -alumina and potash extraction because of the efficient dissociation of muscovite ($\sim 90\%$) within 8 h PBM. The statistically validated experimental responses of Al and K extraction envisaged the optimal conditions of 8 h milling followed by leaching in 2 M HCl at 50°C for 1 h at S:L of 1:20. The milling time was the most influential parameter for both Al and K extraction, and the obtained α -alumina enriched precipitate contains 20% Al_2O_3 with 44.6% recovery and process yield of 27%. The Al_2O_3 -to- SiO_2 ratio in the precipitate is 10.2, with approximately 8–9% silica content and nanocrystalline α -alumina with a surface area of $104.6 \text{ m}^2/\text{g}$. At optimal conditions, the K extraction was 70%, and the K-enriched solution after alumina precipitation can be employed in the fertilizer industry.

ACKNOWLEDGMENTS

The authors acknowledge the funding received from the Science Engineering Research Board, New

Delhi, under extramural funds (EMR/2016/000505) to carry out the research work.

REFERENCES

1. S. Ma, Z. Wen, J. Chen, and S. Zheng, *Miner. Eng.* 22, 793 (2009).
2. R. López-Juárez, N. Razo-Perez, T. Pérez-Juache, O. Hernandez-Cristobal, and S.Y. Reyes-López, *Results Phys.* 11, 1075 (2018).
3. F.M. Kaußen and B. Friedrich, *J. Sustain. Metall.* 2, 353 (2016).
4. V.L. Rayzman, A.V. Aturin, I.Z. Pevzner, V.M. Sizyakov, L.P. Ni, and I.K. Filipovich, *JOM* 55, 47 (2003).
5. IBM, *Indian Minerals Yearbook 2018, (Part 2: Metals and Alloys), 57th Edition: Alumina and Aluminium* (2018).
6. J.T. Klopogge, H.D. Ruan, and R.L. Frost, *J. Mater. Sci.* 37, 1121 (2002).
7. Y. Wang, T. Zhang, G. Lyu, F. Guo, W. Zhang, and Y. Zhang, *J. Clean. Prod.* 188, 456 (2018).
8. E. Dore and H. Hubner (Springer, Berlin, 1984), p. 329.
9. J. Lee, H. Jeon, D.G. Oh, J. Szanyi, and J.H. Kwak, *Appl. Catal. A: General* 500, 58 (2015).
10. M. Chitan, S.A. Hosseini, D. Salari, A. Niaei, and H. Mehrizadeh, *Korean J. Chem. Eng.* 34, 66 (2017).
11. B.L. Cushing, V.L. Kolesnichenko, and C.J. O'Connor, *Chem. Rev.* 104, 3893 (2004).
12. K. Byrappa and M. Yoshimura, *Handbook of Hydrothermal Technology* (Amsterdam: William Andrew, 2012).
13. M.K. Mardkhe, B. Huang, C.H. Bartholomew, T.M. Alam, and B.F. Woodfield, *J. Porous Mater.* 23, 475 (2016).
14. A. Kumar, H. Tanvar, Y. Pratap, and N. Dhawan, *Min. Metall. Explor.* 36, 547 (2019).
15. H. Tanvar and N. Dhawan, *Sep. Sci. Technol.* 55, 1398 (2020).
16. A. Kumar, H. Tanvar, and N. Dhawan, *Trans. Indian Inst. Met.* 73, 23 (2019).
17. Z. Li, Y. Cao, Y. Jiang, G. Han, G. Fan, and L. Chang, *Minerals* 8, 125 (2018).
18. P. Numluk and A. Chaisena, *J. Chem.* 9, 1364 (2012).
19. K.M. Ibrahim, M.K. Moumani, and S.K. Mohammad, *Resources* 7, 63 (2018).
20. Y.F. Adans, A.R. Martins, R.E. Coelho, C.F.D. Virgens, A.D. Ballarini, and L.S. Carvalho, *Mater. Res.* 19, 977 (2016).
21. A. Pehlivan, A.O. Aydin, and A. Alp, *Sak. Univ. J. Sci.* 16, 92 (2012).
22. T. Le, S. Ju, A.V. Ravindra, X. Li, and Q. Wang, *JOM* 71, 831 (2019).
23. S. Agrawal, V. Rayapudi, and N. Dhawan, *Miner. Eng.* 132, 202 (2019).
24. E.R. Bobicki, C.A. Pickles, J. Forster, O. Marzoughi, and R. Hutcheon, *Miner. Eng.* 145, 106055 (2020).
25. H. Tanvar, N. Shukla, and N. Dhawan, *JOM* 72, 823 (2020).
26. A.W. Coats and J.P. Redfern, *Nature* 201, 68 (1964).
27. H.Y. Yu, X.L. Pan, K.W. Dong, W. Zhang, and S.W. Bi, *Advanced Materials Research*, Vol. 616 (Zürich: Trans Tech Publications Ltd, 2013), pp. 1051–1054.
28. C. Guan, L. Chen, Y. Zheng, and W. Sun, *Physicochem. Probl. Miner. Process.* 53, 1038 (2017).
29. J. Ma, Z. Li, and Q. Xiao, *AIChE J.* 58, 2180 (2012).
30. F. Kanwal, A. Batool, M. Adnan, and S. Naseem, *Mater. Res. Innov.* 19, 354 (2015).
31. H.S. Potdar, K.W. Jun, J.W. Bae, S.M. Kim, and Y.J. Lee, *Appl. Catal. A: General* 321, 109 (2007).

Publisher's Note Springer Nature remains neutral with regard to jurisdictional claims in published maps and institutional affiliations.